SUPPORTING INFORMATION

Mechanistic Insights about Electrochemical Proton-Coupled Electron Transfer Derived from a Vibrational Probe

Sohini Sarkar, Anwesha Maitra, William R. Lake, Robert E. Warburton, Sharon Hammes-Schiffer, and Jahan M. Dawlaty

CONTENTS

Computational Methods

We performed periodic DFT calculations on Ag slabs interacting with a MAMBN or MAMBN-H^+ molecule using Quantum ESPRESSO.[1-2] We used the PBE[3] functional both with and without the D3 dispersion correction for these calculations.[4] We find that the computed CN frequencies are similar between the two functionals, but that MAMBN binds more strongly to Ag using the dispersion-corrected PBE-D3 functional, in agreement with trends from previous reports.[5] The core electronic states were treated using the optimized norm-conserving Vanderbilt (ONCV) pseudopotentials,[6-7] and the valence states were expanded in a plane wave basis set up to wave function and charge density energy cutoffs of 60 Ry and 240 Ry, respectively. We employed first-order Methfessel-Paxton smearing[8] of the electronic states with a smearing width of 0.01 Ry. Total energies were converged to 10^{-6} Ry, and the forces on all unconstrained atoms were converged to 10^{-3} Ry/Bohr for geometry optimizations. Since all species in the calculations are closed shell, the results were not sensitive to spin polarization, and all calculations were performed without spin polarization to reduce the computational expense. We found that the nitrile vibrational frequencies were insensitive to reciprocal space sampling, so a single k-point (Γ) was used to generate the potential energy surfaces used in the vibrational analysis. However, we used increased k-point densities in the periodic directions for the adsorption energy, density of states, and crystal orbital Hamilton population (COHP) calculations.

We modeled the solvent using the self-consistent continuum solvation (SCCS) method with the Environ module[2, 9]of Quantum ESPRESSO. In the SCCS method, dielectric continuum solvent is included outside the solute cavity around the surface and molecule in the regions where explicit electron density is not detected. The solvation contribution to the energy is determined by solving the Poisson equation self-consistently with the Kohn-Sham equations. Note that the effects of counterions and ionic strength are not included. In addition to dielectric embedding using the DMSO bulk dielectric constant of 47 for the solvent-exposed side of the slab,[10] a region with $\varepsilon = 1$ corresponding to vacuum was added to the back side of the slab to ensure that charges added or removed from the system were primarily localized on the solvated side

of the slab, where the MAMBN and MAMBN-H^+ molecules were located. We also calculated CN vibrational frequencies for chemisorbed MAMBN on Ag(100) using a region of low dielectric constant (ε = 2.8) near the electrode surface to represent more ordered solvent molecules at the interface.[11-12] The calculated frequencies varied by less than 1 cm^{-1}, and thus we employed dielectric continuum solvation using only the bulk dielectric constant of DMSO. A general schematic of this unit cell setup is shown in Figure S1, and sample Quantum ESPRESSO and Environ input files are provided below.

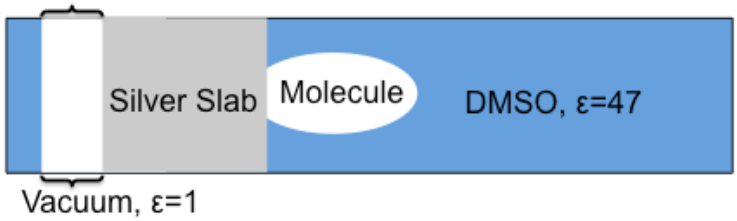

Figure S1. General setup of the dielectric regions in the computational unit cell. Note that the calculation is periodic in all three directions. The side of the slab where the molecule is placed is embedded in dielectric continuum DMSO solvent using the SCCS method. A region of vacuum is added to the back (left) side of the Ag slab to ensure that excess charge localizes on the solvated (right) side.

Models of MAMBN and MAMBN-H^+ near Ag surfaces

We constructed periodic slabs from an optimized bulk Ag structure with a calculated lattice constant of 4.16 Å, in close agreement with the experimentally measured value of 4.08 Å.[13] We used a 4×4 supercell for the Ag(111) and Ag(100) slabs, and a 4×5 supercell for the Ag(322) slab. All slabs were four layers thick, with the bottom two layers fixed to their bulk positions. After the surface was optimized in implicit solvent, the MAMBN or MAMBN-H^+ molecule was optimized in implicit solvent starting from initial configurations at top, bridge, hcp, and fcc sites on the surface. As discussed in the main text, MAMBN-H^+ did not adsorb to the surface, presumably due to the lack of a lone pair on its sp^3 nitrogen. MAMBN-H^+ always optimized to Ag-N distances of 2.9 Å or longer, with a selected geometry shown in Figure S2. MAMBN adsorption, however, is more sensitive to the structure of the slab. For Ag(100) and Ag(322), chemisorbed configurations were observed at top sites with ~2.5 Å distance between the amine

N and the nearest Ag atom. These distances are qualitatively consistent with previous calculations[14-15] and are consistent between the PBE and PBE-D3 functionals used in the present work. Since we did not find a chemisorbed MAMBN species on the Ag(111) surface, we proceeded using the Ag(100) and Ag(322) surfaces for our analysis. The specific configurations considered in this work on Ag(100) and Ag(322) are shown in Figures S2 and S3, respectively. We also computed configurations involving π interactions between the benzonitrile of MAMBN and Ag(100), as shown in Figure S4. These structures optimized to a distance of ~3.3 Å between the benzonitrile and the surface and have a similar adsorption energy (–0.75 eV with PBE-D3) compared to the chemisorbed configuration in Figure S2 (–0.79 eV with PBE-D3. However, this structure is not the configuration that would correspond to the product directly after proton transfer, which requires orientations such as those in Figure S2.

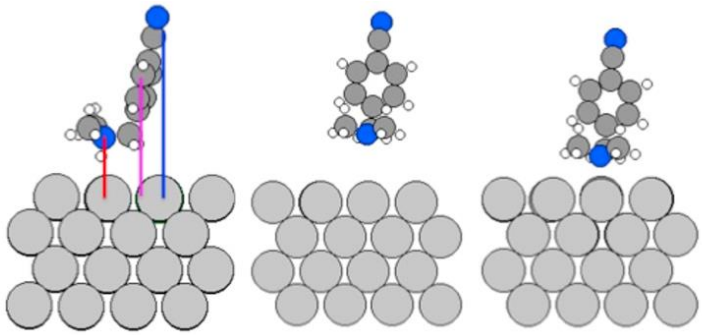

	MAMBN-H$^+$, physisorbed	MAMBN, physisorbed	MAMBN, chemisorbed
Ag-N distance (Å)	3.5	4.1	2.5
Ag-Bz distance (Å)	6.4	7.1	5.9
Ag-CN midpoint (Å)	9.7	11.1	10
Ag-H distance (Å)	2.6	N/A	N/A

Figure S2. Geometries of physisorbed MAMBN-H$^+$ (left), physisorbed MAMBN (center), and chemisorbed MAMBN (right) on Ag(100) computed using the PBE functional. As mentioned in the text, these geometries are similar to those computed using the PBE-D3 functional. The distances from different functional groups of the molecules to the plane of the surface Ag atoms are shown in the accompanying table. The Ag-Bz distance was determined from the center of the ring.

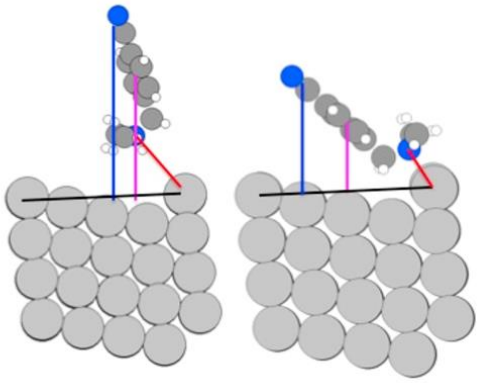

	MAMBN-H$^+$, physisorbed	MAMBN, chemisorbed
Ag-N distance (Å)	4.9	2.5
Ag-Bz distance (Å)	7.3	3.9
Ag-CN midpoint (Å)	10.7	6.0
Ag-H distance (Å)	3.9	N/A

Figure S3. Geometries of physisorbed MAMBN-H$^+$ (left) and chemisorbed MAMBN (right) on Ag(322) computed using the PBE functional. The perpendicular distances from different functional groups of the molecules to the surface plane (indicated by a black line) are shown in the accompanying table.

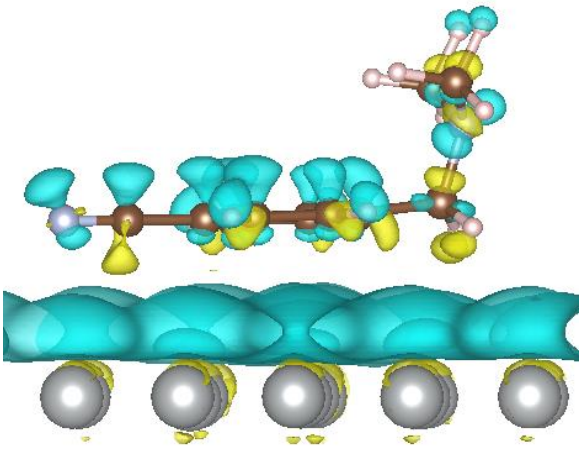

Figure S4. π interactions between Ag(100) and MAMBN. Charge density difference isosurface is shown relative to PZFC at an electrode potential of -0.59 V vs. PZFC at an isosurface level of 0.00025 $e^-/Bohr^3$. The negatively charged Ag electrode causes charge polarization in the benzonitrile group of MAMBN,

leading to a vibrational Stark shift of 3.8 cm^{-1}/V of the nitrile frequency despite it being oriented parallel to the electrode surface.

In addition to the Ag–N bond lengths of ~2.5 Å for the chemisorbed MAMBN configurations on Ag(100) and Ag(322), we performed additional analyses to confirm that these configurations correspond to a chemical bond between the amine N and surface Ag atoms. These results are summarized in Figures S5 and S6 for Ag(100) and Ag(322), respectively. As discussed in the main text, we computed MAMBN adsorption energies of –0.79 eV and –0.98 eV for Ag(100) and Ag(322), respectively, suggesting that MAMBN is weakly bound to these surfaces. The configurations associated with these adsorption energies are shown in Figures S5a and S6a. We also computed the projected density of states (shown in Figures S5b and S6b) and performed COHP analyses using the LOBSTER code[16-20] (shown in Figures S5c and S6c). The COHP analysis projects the Kohn-Sham wave functions from periodic DFT calculations onto localized basis functions representing molecular orbitals. Here, we perform the COHP analysis on the amine N and the Ag atom to which it is coordinated in order to evaluate the electronic populations of Ag–N bonding and antibonding molecular orbitals. Note that a positive value of $-COHP_{Ag-N}$ corresponds to population of a bonding molecular orbital, whereas a negative value corresponds to antibonding molecular orbitals. The overlap in the projected density of states for the amine N and the Ag top site (Figures S5b and S6b) and positive $-COHP_{Ag-N}$ values (Figures S5c and S6c) at similar energy levels suggest that a covalent Ag–N chemical bond is present in these configurations. In both figures, the population of a Ag–N bonding orbital (Figures S5c and S6c) corresponds with occupation of the amine N electronic states (broad blue shaded region between dashed lines in Figures S5b and S6b) and the Ag top site electronic states (dark gray). In contrast, the analogous analysis for the physisorbed MAMBN-H^+ configuration on Ag(100) shown in Figure S2 indicates that a covalent Ag–N chemical bond is not present in this configuration (Figure S7).

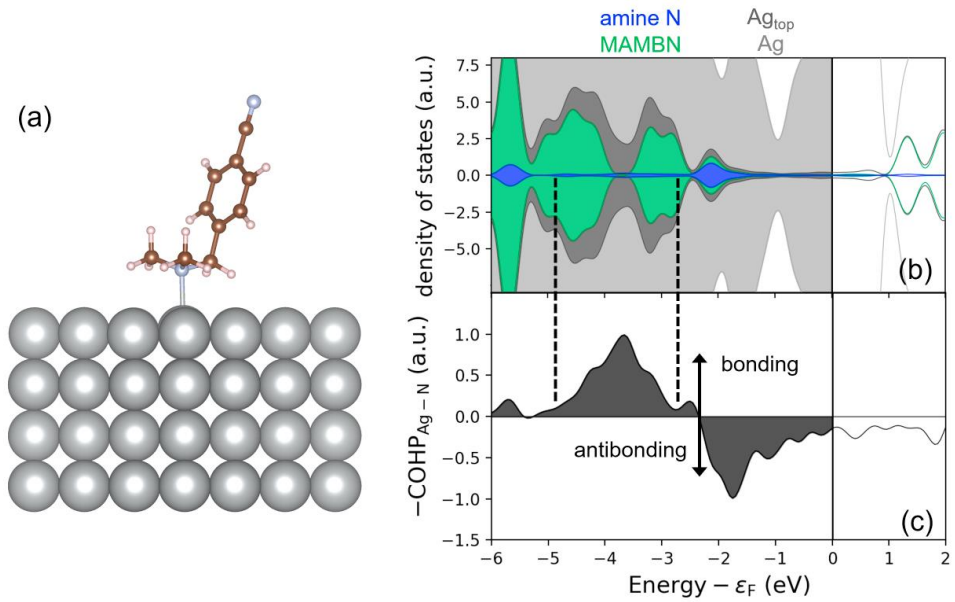

Figure S5. Chemical bonding analysis of MAMBN adsorbed on Ag(100). (a) Configuration of MAMBN adsorbed on the surface, which has an adsorption energy of –0.79 eV. Ag atoms are gray, N atoms are light blue, C atoms are brown, and H atoms are light pink. (b) Atom projected density of states and (c) COHP of the molecular orbital between Ag and the amine N. Ag_{top} denotes the Ag atom that is forming a bond to N, shown in dark gray, and the other Ag atoms are shown in light gray. The energies in (b) and (c) are plotted relative to the Fermi energy ε_F (vertical solid black line). The dashed lines between (b) and (c) are drawn to highlight analogous features associated with the electronic populations of bonding Ag–N molecular orbitals (positive $-COHP_{Ag-N}$ values) and the density of electronic states projected onto these atoms.

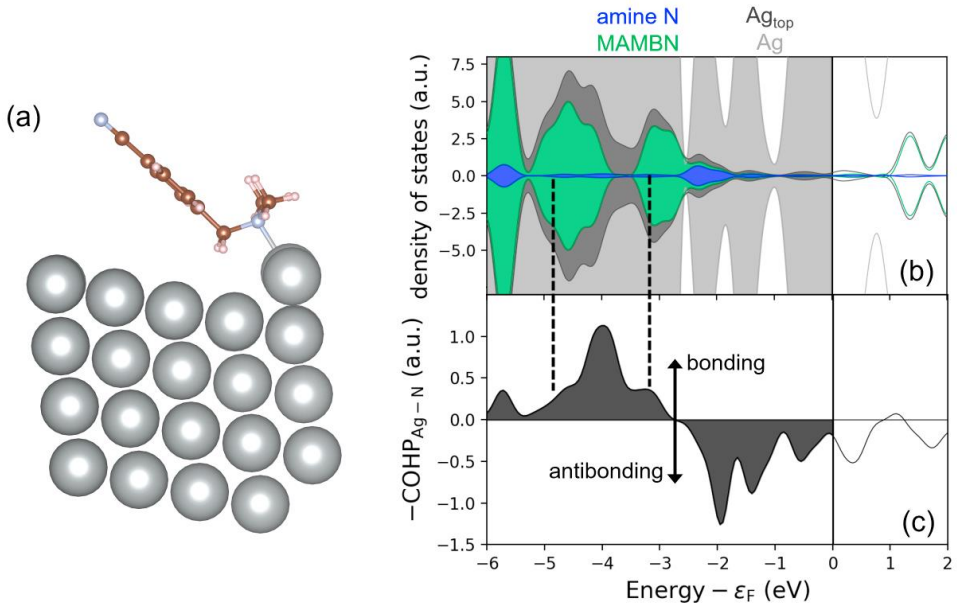

Figure S6. Chemical bonding analysis of MAMBN adsorbed on Ag(322). (a) Configuration of MAMBN adsorbed on the surface, which has an adsorption energy of –0.98 eV. Ag atoms are gray, N atoms are light blue, C atoms are brown, and H atoms are light pink. (b) Atom projected density of states and (c) COHP of the molecular orbital between Ag and the amine N. Ag_{top} denotes the Ag atom that is forming a bond to N, shown in dark gray, and the other Ag atoms are shown in light gray. The energies in (b) and (c) are plotted relative to the Fermi energy ε_F (vertical solid black line). The dashed lines between (b) and (c) are drawn to highlight analogous features associated with the electronic populations of bonding Ag–N molecular orbitals (positive $-COHP_{Ag-N}$ values) and the density of electronic states projected onto these atoms.

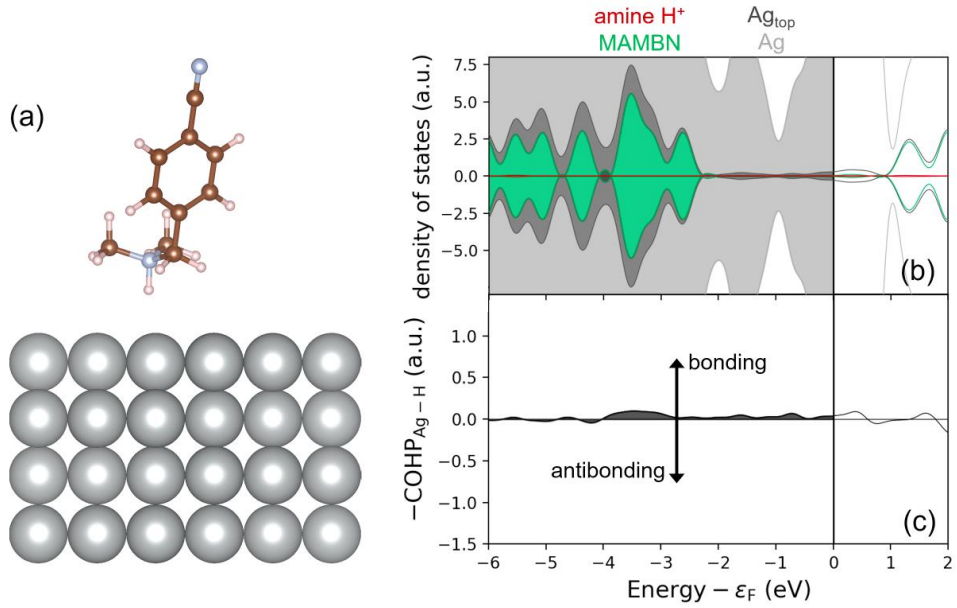

Figure S7. Chemical bonding analysis of MAMBN-H$^+$ on Ag(100). (a) Configuration of MAMBN-H$^+$ near Ag(100). Ag atoms are gray, N atoms are light blue, C atoms are brown, and H atoms are light pink. (b) Atom projected density of states and (c) COHP of the molecular orbital between Ag and the H atom of the terminal amine N. The energies in (b) and (c) are plotted relative to the Fermi energy ε_F (vertical solid black line). The plot in (b) indicates minimal electronic density of states on the H$^+$ of the amine (red data), and the COHP analysis indicates minimal population of Ag–H bonding orbitals. These data suggest that there is no bond formed between Ag and H, and that MAMBN-H$^+$ is physisorbed.

Electrode Potential Calculations and Estimated Reference to Saturated Ag/AgCl Electrode

In this work, we modified the electrode potential by adding and removing electrons from the unit cell. These variable charge calculations are compensated by a homogeneous background charge. In this work, the electrode potential of zero free charge (PZFC) corresponds to conditions where the net charge on the Ag slab is zero. For example, in calculations that contain physisorbed MAMBN-H$^+$, the total charge at PZFC is +1; given that the positive charge is localized mainly on MAMBN-H$^+$, the Ag slab is approximately charge neutral.

To calculate electrode potentials, we reference the Fermi energy, ε_F, to the electrostatic potential in bulk implicit solvent ϕ_{implicit}. However, there is a potential offset between ϕ_{implicit}, the vacuum level ϕ_{vacuum}, and reference electrode potentials (e.g., saturated Ag/AgCl used in the experimental portion of this work).

Hörmann et al. have recently carried out *ab initio* molecular dynamics simulations in implicit H_2O and have shown that there is an intrinsic potential offset of –0.33 V for implicit water versus vacuum.[21] Since our calculations are performed in implicit DMSO, this offset is likely different than that of water. Here, we estimate the analogous offset for implicit DMSO by calculating the difference between ϕ_{implicit} and ϕ_{vacuum} for relaxed Ag(100) surfaces in implicit solvent and in vacuum. This procedure assumes that ε_F is unchanged between solution and vacuum. With these assumptions, we calculate that the intrinsic offset between implicit DMSO and vacuum is ~ –0.76 V. While this approximation may not lead to a quantitatively accurate determination of the offset between ϕ_{implicit} and ϕ_{vacuum}, application of this correction may facilitate comparisons to experimental data. Accounting for the offset between ϕ_{implicit} and ϕ_{vacuum}, as well as the offset between the saturated Ag/AgCl electrode potential[22] and ϕ_{vacuum} of –4.243 V,[23-26] enables estimation of the electrode potentials vs. Ag/AgCl. Overall, this corresponds to an adjustment of the electrode potentials computed in implicit solvent by –3.48 V to put them on the Ag/AgCl scale. The figures in this paper are plotted versus PZFC, but this analysis enables the reader to shift the calculated results to the Ag/AgCl scale. For reference, the computed PZFC values with respect to implicit solvent are 3.38 V, 3.42 V, and 3.56 V for the chemisorbed MAMBN, physisorbed MAMBN, and physisorbed MAMBN-H^+, respectively.

Computational Vibrational Analysis of Nitrile Stretch

For benchmarking purposes, we calculated the nitrile stretch vibrational frequencies within the harmonic approximation by computing and diagonalizing the Hessian. The Hessian calculations were performed on gas phase MAMBN and MAMBN-H^+ molecules using the PBE functional and the phonon module in Quantum ESPRESSO. After each geometry was optimized, we verified that all eigenvalues corresponding to vibrations were positive to confirm that the geometry corresponds to a minimum. The normal mode vectors were obtained from Hessian calculations using the PBE functional, but these normal mode vectors were found to be virtually identical to those obtained using the PBE-D3 functional (i.e., the dot product of the normal mode vectors computed using PBE and PBE-D3 in Quantum ESPRESSO were

nearly unity (> 0.99). These frequencies were compared to analogous Hessian calculations using the 6-31+G** basis set and the B3LYP-D3[4, 27-28] and ωB97XD[29] functionals computed in implicit solvent with the Gaussian16 code[30] We found that the relative nitrile vibrational frequencies (Table S1) and the corresponding normal mode coordinates for MAMBN and MAMBN-H^+ are qualitatively similar at these various levels of theory. The normal modes from the gas phase PBE calculations in Quantum ESPRESSO are given in Tables S2 and S3, respectively. Example input files are also provided below.

Table S1. Nitrile Stretch Frequencies (cm^{-1}) of MAMBN and MAMBN-H^+ Obtained Experimentally and Computationally

		ν_{CN} unprotonated	ν_{CN} protonated	$\Delta\nu_{CN}$
Experimental (Pure)		2229	2236	+7
Computation				
B3LYP-D3/6-31+G** implicit DMSO	Harmonic	2319	2330	+11
	FGH	2292	2303	+11
ωB97XD/6-31+G** implicit DMSO	Harmonic	2367	2376	+11
	FGH	2341	2351	+10
PBE vacuum	Harmonic	2222	2236	+11
	FGH	2209	2215	+6
PBE implicit DMSO	FGH	2191	2209	+18
PBE-D3 vacuum	Harmonic	2226	2239	+13
	FGH	2209	2227	+18
PBE-D3 implicit DMSO	FGH	2191	2206	+15
PBE physisorbed near Ag(100) in DMSO	FGH	2191	2200	+9
PBE chemisorbed on Ag(100) in DMSO	FGH	2193	N/A	N/A
PBE-D3 physisorbed near Ag(100) in DMSO	FGH	2195	2203	+8
PBE-D3 chemisorbed on Ag(100) in DMSO	FGH	2193	N/A	N/A
PBE-D3 π interaction between benzonitrile and Ag(100)	FGH	2184	2191	+7

Table S2. Normal Mode Coordinates and Reduced Mass for MAMBN-H^+ Nitrile Stretching Mode Calculated in Vacuum with PBE Functional

Normal Mode Reduced Mass:	12.67 au		
	Normal Mode Coordinates		
Atom Type	X	Y	Z
C	0.004268	-0.018339	0.123311
C	-0.0053	-0.001589	0.014514
C	-0.002111	0.001623	-0.010309
C	0.000071	-0.000759	0.004831
C	0.001374	0.001313	-0.010421
C	0.006572	-0.002599	0.013755
H	0.007357	0.000207	-0.00318
H	0.005132	-0.000065	-0.004325
H	-0.005526	0.001152	-0.003848
H	-0.007663	0.000452	-0.000552
C	-0.028899	0.118759	-0.79612
C	0.000066	0.000767	0.00000
H	-0.000747	0.000245	-0.000854
H	0.00065	0.000031	-0.000813
N	-0.000006	0.000139	-0.000657
C	0.000531	-0.000041	0.000011
H	-0.000565	-0.001938	-0.00207
H	-0.000196	-0.000773	0.000542
H	-0.000938	-0.000437	0.00294
C	-0.000429	0.000002	0.000088
H	0.000402	-0.000892	0.000389
H	-0.000385	-0.001741	-0.002185
H	-0.000241	0.000328	0.000594

Table S3. Normal Mode Coordinates and Reduced Mass for MAMBN Nitrile Stretching Mode Calculated in Vacuum with PBE Functional

Normal Mode Reduced Mass:			12.64 au
	Normal Mode Coordinates		
Atom Type	X	Y	Z
C	0.002355	0.018598	0.126907
C	0.005644	0.000151	0.012124
C	0.00207	-0.001915	-0.009053
C	-0.000533	0.000696	0.004491
C	-0.001928	-0.000831	-0.008571
C	-0.006082	0.003163	0.011036
H	-0.011733	0.001196	-0.008227
H	-0.002008	-0.000631	-0.012367
H	0.00328	-0.005315	-0.010733
H	0.017424	-0.004322	-0.012792
C	-0.01132	-0.114077	-0.795745
C	-0.000485	-0.001394	0.001601
H	-0.004592	0.006831	-0.005362
H	0.007463	-0.004379	-0.004555
N	0.000455	0.001278	0.001846
C	0.00012	0.001121	0.002224
H	-0.005869	0.006534	-0.006925
H	-0.002579	-0.011456	0.001564
H	-0.006012	0.010426	-0.013609
C	-0.001134	0.00233	0.001002
H	-0.018679	-0.005997	0.004988
H	0.002778	0.001292	-0.008635
H	0.006578	-0.011797	-0.001696
N	0.007885	0.080444	0.572095
H	-0.003774	-0.016243	-0.007439

For comparison to the experimental data, we calculated the nitrile stretch vibrational frequencies using a grid-based method that includes anharmonic effects. The grid for the surface-molecule system was generated along the normal mode vector corresponding to the nitrile stretch computed from the Hessian calculations described above for the gas phase molecules (Tables S2 and S3). In practice, these gas phase normal modes were defined in Cartesian coordinates relative to the gas phase optimized geometry. To superimpose the gas phase geometry onto the MAMBN or MAMBN-H^+ geometry optimized near the model

Ag surface, we translated the gas phase molecule so that the benzene carbon atom bound to the nitrile carbon was overlaid on its surface-molecule counterpart. Then we rotated the nitrile carbon of the gas phase molecule and the carbon alpha to the nitrile into their respective surface-molecule counterparts. The product of these two rotational transformations defines a rotation matrix, which was used to rotate the gas phase normal mode coordinates to be consistent with the orientation of MAMBN or MAMBN-H^+ near the Ag surface.

A series of single-point energy calculations were performed for grid points along this normal mode vector to generate the anharmonic potential energy curve corresponding to the nitrile stretch. Nine grid points separated by 0.05 Å, corresponding to a total sampling length of 0.4 Å, were used to generate this potential energy curve. Each grid point used a single k-point in all directions, as including more k-points was determined to have an impact of less than 1 cm^{-1} on the nitrile stretching frequency (Table S4). A spline procedure was then used to generate a potential energy curve represented by 801 grid points over this length (convergence information in Table S5). After generating this potential energy curve, the Fourier grid Hamiltonian (FGH) method[31] was used to solve the one-dimensional Schrödinger equation using the mass associated with the nitrile stretch normal mode computed for the gas phase molecule. The vibrational frequencies reported are the energy differences between the ground and first excited vibrational states. Doubling the number of computed points within the same sampling length (i.e., doubling the density) or doubling the total sampling length with the same grid point separation changed the vibrational frequencies by less than 1 cm^{-1} (Table S4).

Table S4. Benchmarking for the FGH Calculations of the Nitrile Frequencies for Chemisorbed MAMBN on Ag(100) with Respect to the Number of Computed Grid Points and k-Points

Sampling Length (Å)	Grid Spacing (Å)	k-points	Nitrile Frequency (cm^{-1})
0.4	0.05	(1 1 1)	2193.3
0.4	0.025	(1 1 1)	2193.32
0.8	0.05	(1 1 1)	2193.3
0.4	0.05	(2 2 1)	2193
0.4	0.05	(3 3 1)	2192.82

Table S5. Benchmarking for the FGH Calculations of the Nitrile Frequencies for Chemisorbed MAMBN on Ag(100) with Respect to the Number of Grid Points after the Spline Procedure

Number of Grid Points after Spline	Nitrile Frequency (cm^{-1})
81	2188
801	2193
8001	2193

To evaluate the Stark shifts of the MAMBN and MAMBN-H^+ molecules near the Ag surfaces, we computed the nitrile stretch frequencies as a function of applied potential. As described above, we applied a potential bias to the electrode by adding or removing electrons, where any net charge on the unit cell is compensated by a homogeneous background charge. For any given electrode potential, the charge of the unit cell is constant. Therefore, any energetic corrections associated with a charged unit cell will be effectively constant for all CN distances along the potential energy curve and will not affect the calculated CN vibrational frequencies. In addition to the Stark shift calculations presented in Figure 7 (left panel) of the main text, Figure S8 shows analogous results for additional configurations for MAMBN and MAMBN-H^+ near Ag(100) and Ag(322).

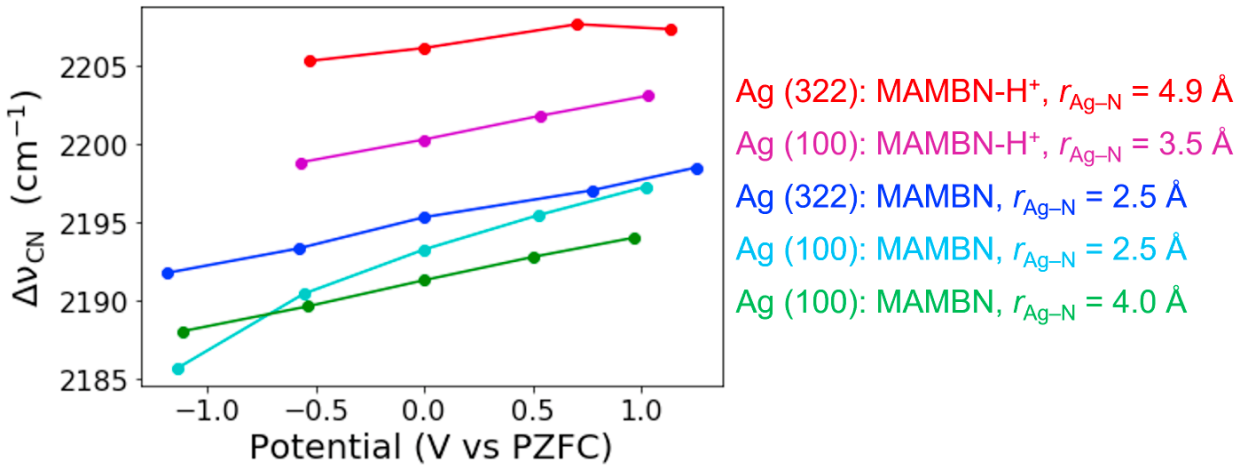

Figure S8. Calculated vibrational frequencies (PBE) versus potential for different MAMBN and MAMBN-H$^+$ configurations near Ag(100) and Ag(322). For equivalent structures, the slope is smaller when r_{Ag-N} is larger (compare cyan and green curves). The chemisorbed MAMBN on Ag(322) has a smaller slope than expected because of its tilted orientation (Figure S3).

Bader Charge Analysis

To ensure that added charge is localized on the Ag slab and not the molecule, we performed Bader charge analyses[32-34] on three Ag(100) systems using the PBE functional: MAMBN chemisorbed, MAMBN physisorbed, and MAMBN-H$^+$ physisorbed. The analyses are shown in Figure S9, corresponding to the configurations shown above in Figure S2. Figure S9 shows that there is minimal charge transfer to the physisorbed MAMBN, implying that all excess charge is localized on Ag. This analysis indicates some charge transfer between Ag(100) and chemisorbed MAMBN with applied potential. As discussed in the main text, this small degree of charge transfer is presumably because the amine nitrogen is covalently bound to the Ag surface (also shown in Figure S5). At more negative potentials, there is charge transfer to the physisorbed MAMBN-H$^+$, suggesting that the proton is likely to be discharged to the Ag surface at these potentials, i.e., MAMBN-H$^+$ is not reductively stable. This analysis further suggests that the changes in the charge density difference isosurfaces across the benzene and nitrile in Figure 5 of the main text are primarily due to polarization of the charge by the interfacial field, and not charge transfer from Ag to the molecule.

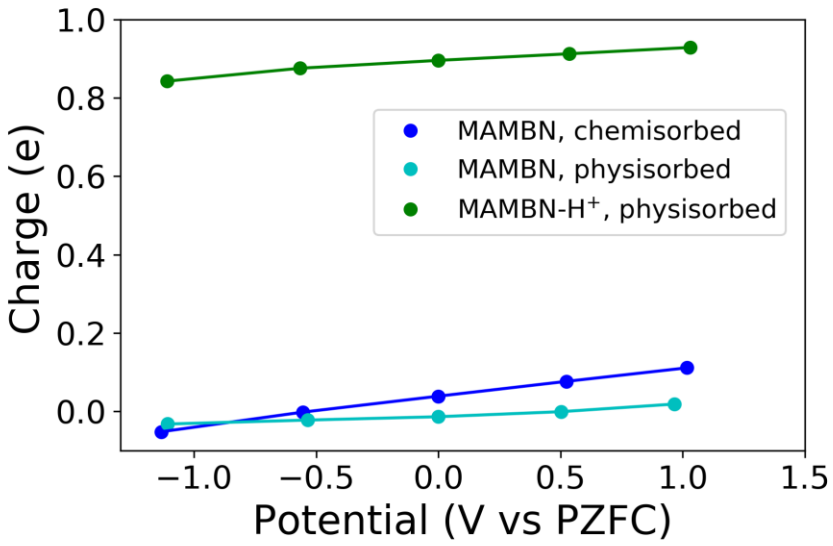

Figure S9. Bader charges of MAMBN chemisorbed and physisorbed and MAMBN-H^+ physisorbed configurations on Ag(100) for different applied potentials.

Sample Input Files and Selected Geometric Coordinates

Calculation input file of MAMBN-H^+ on Ag(100) at PZFC

```
&control
   calculation = 'scf'
   pseudo_dir = '/home/wl447/project/planewave_setup/pseudo/ONCV/'
   outdir = './'
   title = 'proton_sur_scf'
   prefix = 'proton_sur_scf'
   ! wf_collect = .true.
   nstep = 499
   tefield = .false.
   ! dipfield = .true.
 /
&SYSTEM
   ntyp = 4,
   nat = 89,
   ibrav = 0
   ecutwfc = 60,
   tot_charge = 1
   nspin = 1
   starting_magnetization(1) = 0.0
   smearing = 'mp'
   degauss = 0.01
   occupations = 'smearing'
   input_dft = 'pbe'
   nosym = .true.
 /
&electrons
   startingpot = 'file'
   ! startingwfc = 'file'
   ! mixing_mode = 'local-TF'
   mixing_beta = 0.1,
   mixing_ndim = 12,
   mixing_fixed_ns = 12,
   electron_maxstep=50000,
   conv_thr =  1.0d-6
   diago_full_acc =.true.
   adaptive_thr = .true.
 /
&ions
   ion_dynamics= 'bfgs'
 /
K_POINTS 7
2 2 1 0 0 0
ATOMIC_SPECIES
Ag 107.87 Ag_ONCV_PBE-1.0.upf
N   14.01 N_ONCV_PBE-1.0.upf
C   12.01 C_ONCV_PBE-1.0.upf
H    1.01 H_ONCV_PBE-1.0.upf
CELL_PARAMETERS (angstrom)
```

```
  11.7286387582 0.000000000    0.000000000
  0.000000000   11.7286387582  0.000000000
  0.000000000   0.000000000    50.00000000
ATOMIC_POSITIONS (angstrom)
Ag      1.466079840   1.466079840  10.000000000   0   0   0
Ag      4.398239530   1.466079840  10.000000000   0   0   0
Ag      7.330399220   1.466079840  10.000000000   0   0   0
Ag     10.262558910   1.466079840  10.000000000   0   0   0
Ag      1.466079840   4.398239530  10.000000000   0   0   0
Ag      4.398239530   4.398239530  10.000000000   0   0   0
Ag      7.330399220   4.398239530  10.000000000   0   0   0
Ag     10.262558910   4.398239530  10.000000000   0   0   0
Ag      1.466079840   7.330399220  10.000000000   0   0   0
Ag      4.398239530   7.330399220  10.000000000   0   0   0
Ag      7.330399220   7.330399220  10.000000000   0   0   0
Ag     10.262558910   7.330399220  10.000000000   0   0   0
Ag      1.466079840  10.262558910  10.000000000   0   0   0
Ag      4.398239530  10.262558910  10.000000000   0   0   0
Ag      7.330399220  10.262558910  10.000000000   0   0   0
Ag     10.262558910  10.262558910  10.000000000   0   0   0
Ag      0.000000000   0.000000000  12.073350000   0   0   0
Ag      2.932159690   0.000000000  12.073350000   0   0   0
Ag      5.864319380   0.000000000  12.073350000   0   0   0
Ag      8.796479070   0.000000000  12.073350000   0   0   0
Ag      0.000000000   2.932159690  12.073350000   0   0   0
Ag      2.932159690   2.932159690  12.073350000   0   0   0
Ag      5.864319380   2.932159690  12.073350000   0   0   0
Ag      8.796479070   2.932159690  12.073350000   0   0   0
Ag      0.000000000   5.864319380  12.073350000   0   0   0
Ag      2.932159690   5.864319380  12.073350000   0   0   0
Ag      5.864319380   5.864319380  12.073350000   0   0   0
Ag      8.796479070   5.864319380  12.073350000   0   0   0
Ag      0.000000000   8.796479070  12.073350000   0   0   0
Ag      2.932159690   8.796479070  12.073350000   0   0   0
Ag      5.864319380   8.796479070  12.073350000   0   0   0
Ag      8.796479070   8.796479070  12.073350000   0   0   0
Ag      1.465706325   1.466030374  14.129159791
Ag      4.396730356   1.464344336  14.131358297
Ag      7.330456988   1.463925883  14.130907046
Ag     10.261888674   1.466189770  14.129745512
Ag      1.465143363   4.396854222  14.130620037
Ag      4.392464650   4.390959695  14.118632793
Ag      7.339828093   4.389561042  14.117183402
Ag     10.266663419   4.397629947  14.131218378
Ag      1.465492740   7.331996476  14.130964675
Ag      4.392592315   7.337525748  14.118780008
Ag      7.340129642   7.338930338  14.117506765
Ag     10.267149981   7.331176952  14.131623527
Ag      1.466009642  10.262649684  14.129374014
Ag      4.396903102  10.265011258  14.131276163
Ag      7.331113242  10.265132645  14.131124177
```

Ag	10.262512300	10.262266801	14.130155353
Ag	-0.001205839	0.000086232	16.133526254
Ag	2.927155465	0.000408049	16.134257275
Ag	5.861358290	0.000836479	16.130975282
Ag	8.796990599	0.000323162	16.133109212
Ag	0.000782577	2.929226338	16.133446393
Ag	2.932227548	2.931323076	16.136853540
Ag	5.865972070	2.943372322	16.126058739
Ag	8.797705506	2.931825294	16.136900123
Ag	0.002703582	5.864247443	16.131398176
Ag	2.945415581	5.863924863	16.121753503
Ag	5.871981701	5.863689377	16.096847795
Ag	8.787947465	5.864111101	16.124995450
Ag	0.002144757	8.799472083	16.134517052
Ag	2.933140827	8.797658295	16.137016713
Ag	5.866341522	8.785892050	16.124499179
Ag	8.798726418	8.796614115	16.137070110
C	3.50828920	6.51672238	24.01533590
C	3.48978064	5.25741514	23.39451118
C	3.87575047	5.14490988	22.06499096
C	4.28800031	6.27205095	21.34148310
C	4.28306677	7.52615571	21.96613289
C	3.90060389	7.65616083	23.29489507
H	3.17040342	4.38013294	23.95147953
H	3.84256166	4.16906208	21.58333469
H	4.57012149	8.41550641	21.40669068
H	3.89851301	8.63172644	23.77516683
C	3.12022136	6.63734195	25.38199752
C	4.67581313	6.14634175	19.89609445
H	4.14586830	5.31761814	19.41378178
H	4.45832427	7.07050227	19.34882232
N	6.16052261	5.87592160	19.66040190
C	7.04360001	6.99501297	20.11396165
H	6.99740288	7.05625127	21.20328130
H	8.06615769	6.77441206	19.79713046
H	6.69689928	7.92802301	19.66161985
C	6.61901817	4.55846569	20.20199197
H	7.65070474	4.39736329	19.87934220
H	6.57237896	4.59294907	21.29234016
H	5.97093632	3.76825395	19.81400997
N	2.80683820	6.73162450	26.49897322
H	6.25183262	5.82262130	18.62450966

Geometry of MAMBN-H^+ on Ag(111)

Ag	0.000000000	0.000000000	10.000000000	0	0	0
Ag	2.892066740	0.000000000	10.000000000	0	0	0
Ag	5.784133470	0.000000000	10.000000000	0	0	0
Ag	8.676200210	0.000000000	10.000000000	0	0	0
Ag	1.446033370	2.504603260	10.000000000	0	0	0
Ag	4.338100100	2.504603260	10.000000000	0	0	0
Ag	7.230166840	2.504603260	10.000000000	0	0	0

Ag 10.122233570 2.504603260 10.000000000 0 0 0
Ag 0.000000000 5.009206520 10.000000000 0 0 0
Ag 2.892066740 5.009206520 10.000000000 0 0 0
Ag 5.784133470 5.009206520 10.000000000 0 0 0
Ag 8.676200210 5.009206520 10.000000000 0 0 0
Ag 1.446033370 7.513809790 10.000000000 0 0 0
Ag 4.338100100 7.513809790 10.000000000 0 0 0
Ag 7.230166840 7.513809790 10.000000000 0 0 0
Ag 10.122233570 7.513809790 10.000000000 0 0 0
Ag 1.446033370 0.834867750 12.361362600 0 0 0
Ag 4.338100100 0.834867750 12.361362600 0 0 0
Ag 7.230166840 0.834867750 12.361362600 0 0 0
Ag 10.122233570 0.834867750 12.361362600 0 0 0
Ag 0.000000000 3.339471020 12.361362600 0 0 0
Ag 2.892066740 3.339471020 12.361362600 0 0 0
Ag 5.784133470 3.339471020 12.361362600 0 0 0
Ag 8.676200210 3.339471020 12.361362600 0 0 0
Ag 1.446033370 5.844074280 12.361362600 0 0 0
Ag 4.338100100 5.844074280 12.361362600 0 0 0
Ag 7.230166840 5.844074280 12.361362600 0 0 0
Ag 10.122233570 5.844074280 12.361362600 0 0 0
Ag 0.000000000 8.348677540 12.361362600 0 0 0
Ag 2.892066740 8.348677540 12.361362600 0 0 0
Ag 5.784133470 8.348677540 12.361362600 0 0 0
Ag 8.676200210 8.348677540 12.361362600 0 0 0
Ag 0.00000000 1.66973551 14.72272520
Ag 2.89206674 1.66973551 14.72272520
Ag 5.78413347 1.66973551 14.72272520
Ag 8.67620021 1.66973551 14.72272520
Ag 1.44603337 4.17433877 14.72272520
Ag 4.33810010 4.17433877 14.72272520
Ag 7.23016684 4.17433877 14.72272520
Ag 10.12223357 4.17433877 14.72272520
Ag 0.00000000 6.67894203 14.72272520
Ag 2.89206674 6.67894203 14.72272520
Ag 5.78413347 6.67894203 14.72272520
Ag 8.67620021 6.67894203 14.72272520
Ag 1.44603337 9.18354529 14.72272520
Ag 4.33810010 9.18354529 14.72272520
Ag 7.23016684 9.18354529 14.72272520
Ag 10.12223357 9.18354529 14.72272520
Ag 0.00000000 0.00000000 17.08408780
Ag 2.89206674 0.00000000 17.08408780
Ag 5.78413347 0.00000000 17.08408780
Ag 8.67620021 0.00000000 17.08408780
Ag 1.44603337 2.50460326 17.08408780
Ag 4.33810010 2.50460326 17.08408780
Ag 7.23016684 2.50460326 17.08408780
Ag 10.12223357 2.50460326 17.08408780
Ag 0.00000000 5.00920652 17.08408780
Ag 2.89206674 5.00920652 17.08408780

Ag 5.78413347 5.00920652 17.08408780
Ag 8.67620021 5.00920652 17.08408780
Ag 1.44603337 7.51380979 17.08408780
Ag 4.33810010 7.51380979 17.08408780
Ag 7.23016684 7.51380979 17.08408780
Ag 10.12223357 7.51380979 17.08408780
C 3.56448510 5.61413947 24.31630402
C 3.47476023 4.36900216 23.67354871
C 3.74227420 4.27381826 22.31443847
C 4.10809069 5.40777277 21.57464455
C 4.17145125 6.65130875 22.22047158
C 3.90791416 6.75898292 23.57960786
H 3.18435176 3.48872628 24.24333883
H 3.64005213 3.30623651 21.82194286
H 4.40494540 7.55351313 21.65418259
H 3.95186404 7.72591440 24.07662051
C 3.29203247 5.71908133 25.71217053
C 4.37062328 5.30055870 20.10431952
H 3.81262610 4.47121090 19.65297028
H 4.11161719 6.22674560 19.57691906
N 5.84907736 5.03281916 19.73832750
C 6.76173524 6.15578687 20.12903954
H 6.76154504 6.24228616 21.21870050
H 7.76971413 5.92892057 19.76947626
H 6.40169732 7.08425202 19.67606670
C 6.34992320 3.71805225 20.25537457
H 7.37153894 3.56650608 19.89466949
H 6.33629796 3.74511293 21.34800376
H 5.69990537 2.91801187 19.88901011
N 3.07563314 5.80459890 26.85131937
H 5.86235939 4.97780446 18.71252238

Geometry of MAMBN-H^+ on Ag(322)

Ag	5.230262120	3.448978770	10.000128290	0	0	0
Ag	3.505068410	1.077927380	10.000128290	0	0	0
Ag	8.105566330	3.170048290	10.502853740	0	0	0
Ag	6.380372620	0.798996900	10.502853740	0	0	0
Ag	10.980836030	2.891070380	11.005874730	0	0	0
Ag	9.255642330	0.520018990	11.005874730	0	0	0
Ag	13.856289760	2.612139900	11.508600180	0	0	0
Ag	12.131096050	0.241088510	11.508600180	0	0	0
Ag	1.779859460	2.333161990	12.011621170	0	0	0
Ag	3.505053170	4.704213380	12.011621170	0	0	0
Ag	4.655163670	2.054231500	12.514346620	0	0	0
Ag	6.380357380	4.425282890	12.514346620	0	0	0
Ag	7.530467880	1.775301020	13.017367620	0	0	0
Ag	9.255661590	4.146352410	13.017367620	0	0	0
Ag	10.405737580	1.496323110	13.520093060	0	0	0
Ag	12.130931290	3.867374500	13.520093060	0	0	0
Ag	13.281191310	1.217392630	14.023114060	0	0	0
Ag	15.006385020	3.588444020	14.023114060	0	0	0

Ag	1.204795520	0.938462140	14.525839500	0	0	0
Ag	2.929989230	3.309513530	14.525839500	0	0	0
Ag	8.680649540	8.191081550	10.000128290	0	0	0
Ag	6.955455830	5.820030160	10.000128290	0	0	0
Ag	11.555953750	7.912151070	10.502853740	0	0	0
Ag	9.830760040	5.541099680	10.502853740	0	0	0
Ag	14.431223450	7.633173160	11.005874730	0	0	0
Ag	12.706029750	5.262121770	11.005874730	0	0	0
Ag	17.306677180	7.354242680	11.508600180	0	0	0
Ag	15.581483470	4.983191290	11.508600180	0	0	0
Ag	5.230246880	7.075264770	12.011621170	0	0	0
Ag	6.955440590	9.446316160	12.011621170	0	0	0
Ag	8.105551090	6.796334280	12.514346620	0	0	0
Ag	9.830744800	9.167385670	12.514346620	0	0	0
Ag	10.980855300	6.517403800	13.017367620	0	0	0
Ag	12.706049010	8.888455190	13.017367620	0	0	0
Ag	13.856125000	6.238425890	13.520093060	0	0	0
Ag	15.581318710	8.609477280	13.520093060	0	0	0
Ag	16.731578730	5.959495410	14.023114060	0	0	0
Ag	18.456772440	8.330546800	14.023114060	0	0	0
Ag	4.655182940	5.680564920	14.525839500	0	0	0
Ag	6.380376650	8.051616310	14.525839500	0	0	0
Ag	4.087272004	0.655547242	15.008613359			
Ag	5.820192635	3.021576507	15.000188153			
Ag	6.947213376	0.381754414	15.515694786			
Ag	8.667201217	2.753709113	15.510784350			
Ag	9.820296068	0.094841503	15.993390709			
Ag	11.552243283	2.462845940	15.994728738			
Ag	16.157785737	4.553557174	16.500742264			
Ag	14.424434357	2.183212180	16.505790104			
Ag	4.091790434	4.263476528	16.999897624			
Ag	2.371884874	1.893886158	16.992582101			
Ag	6.957886031	3.999853696	17.591499159			
Ag	5.237378625	1.628568859	17.580340703			
Ag	9.828674420	3.723634007	18.006836101			
Ag	8.092048628	1.348065770	18.016435350			
Ag	12.667532999	3.468117108	18.511839122			
Ag	10.927156941	1.097807392	18.514399124			
Ag	15.488452930	3.217535420	19.034772590			
Ag	13.756723678	0.860465245	19.033999072			
Ag	3.376322417	2.976958984	19.421712356			
Ag	1.641910572	0.607875624	19.405150472			
Ag	7.532189195	5.397175134	15.007122805			
Ag	9.261352476	7.770085600	15.007163036			
Ag	10.392805626	5.126502121	15.517063525			
Ag	12.121433461	7.493529741	15.516245698			
Ag	13.286991061	4.830482190	16.004583765			
Ag	14.996339471	7.204561223	15.998763283			
Ag	19.596307538	9.298762676	16.500274603			
Ag	17.875917580	6.936966466	16.502423784			
Ag	7.543354238	9.018308759	16.989218672			

Ag	5.821703181	6.646238665	16.995725305
Ag	10.410640679	8.744844256	17.574015771
Ag	8.687811067	6.376472609	17.586097543
Ag	13.266805128	8.465990309	18.019632950
Ag	11.559544338	6.103087599	18.018527988
Ag	16.106030729	8.219225319	18.519498786
Ag	14.388602357	5.839825206	18.516094629
Ag	18.927683721	7.983627022	19.049712052
Ag	17.199660683	5.599837655	19.041828797
Ag	6.806102941	7.720308053	19.420080444
Ag	5.061173455	5.361225800	19.368484385
C	11.788470373	4.052988724	23.826319518
C	11.492010053	5.341170754	23.346492343
C	10.421136438	5.511285188	22.481535551
C	9.635345305	4.418563495	22.089882332
C	9.961949440	3.133699987	22.549909487
C	11.030113741	2.943786742	23.415614552
H	12.101300662	6.192232456	23.651430266
H	10.204238293	6.503935347	22.088223210
H	9.386370945	2.274314379	22.211698385
H	11.284066029	1.944940259	23.771228725
C	12.864934716	3.872536543	24.741224150
C	8.499515035	4.611207981	21.133888122
H	8.684990153	5.471111946	20.471772204
H	8.355425441	3.720508108	20.502954701
N	7.154711885	4.879087991	21.793680355
C	6.625431240	3.714574273	22.562787979
H	7.265597053	3.548974395	23.430639880
H	5.608526703	3.947498274	22.883162957
H	6.616606052	2.833509462	21.918820459
C	7.123999522	6.135372780	22.602064071
H	6.093703619	6.314954251	22.918645814
H	7.782754362	6.015201248	23.464692696
H	7.467003820	6.965674488	21.974755458
N	13.747379707	3.726131499	25.486080337
H	6.498321597	5.032133117	20.984288064

Geometry of MAMBN on Ag(100)

Ag 1.46607984 1.46607984 10.00000000 0 0 0
Ag 4.39823953 1.46607984 10.00000000 0 0 0
Ag 7.33039922 1.46607984 10.00000000 0 0 0
Ag 10.26255891 1.46607984 10.00000000 0 0 0
Ag 1.46607984 4.39823953 10.00000000 0 0 0
Ag 4.39823953 4.39823953 10.00000000 0 0 0
Ag 7.33039922 4.39823953 10.00000000 0 0 0
Ag 10.26255891 4.39823953 10.00000000 0 0 0
Ag 1.46607984 7.33039922 10.00000000 0 0 0
Ag 4.39823953 7.33039922 10.00000000 0 0 0
Ag 7.33039922 7.33039922 10.00000000 0 0 0
Ag 10.26255891 7.33039922 10.00000000 0 0 0
Ag 1.46607984 10.26255891 10.00000000 0 0 0

Ag 4.39823953 10.26255891 10.00000000 0 0 0
Ag 7.33039922 10.26255891 10.00000000 0 0 0
Ag 10.26255891 10.26255891 10.00000000 0 0 0
Ag 0.00000000 0.00000000 12.07335000 0 0 0
Ag 2.93215969 0.00000000 12.07335000 0 0 0
Ag 5.86431938 0.00000000 12.07335000 0 0 0
Ag 8.79647907 0.00000000 12.07335000 0 0 0
Ag 0.00000000 2.93215969 12.07335000 0 0 0
Ag 2.93215969 2.93215969 12.07335000 0 0 0
Ag 5.86431938 2.93215969 12.07335000 0 0 0
Ag 8.79647907 2.93215969 12.07335000 0 0 0
Ag 0.00000000 5.86431938 12.07335000 0 0 0
Ag 2.93215969 5.86431938 12.07335000 0 0 0
Ag 5.86431938 5.86431938 12.07335000 0 0 0
Ag 8.79647907 5.86431938 12.07335000 0 0 0
Ag 0.00000000 8.79647907 12.07335000 0 0 0
Ag 2.93215969 8.79647907 12.07335000 0 0 0
Ag 5.86431938 8.79647907 12.07335000 0 0 0
Ag 8.79647907 8.79647907 12.07335000 0 0 0
Ag 1.466629510 1.465613914 14.185146457
Ag 4.397875463 1.463661875 14.185979442
Ag 7.330845055 1.464581761 14.187247515
Ag 10.263272505 1.465730998 14.185232845
Ag 1.469751761 4.397554259 14.187658626
Ag 4.403127021 4.397237483 14.188038701
Ag 7.331018554 4.397780331 14.188875071
Ag 10.264483876 4.398150591 14.186620101
Ag 1.469644014 7.330972334 14.187037070
Ag 4.403099178 7.325920074 14.187457667
Ag 7.331307559 7.325615443 14.188041752
Ag 10.264908283 7.330537995 14.186145566
Ag 1.466899774 10.261876232 14.185406498
Ag 4.397811452 10.259802267 14.186095794
Ag 7.331073604 10.259140502 14.187541116
Ag 10.263259039 10.262007427 14.185430965
Ag -0.000432065 0.000637704 16.299150593
Ag 2.935970187 -0.001748895 16.301920701
Ag 5.865471260 -0.007854020 16.304759938
Ag 8.794352256 -0.001588836 16.302525934
Ag 0.001408694 2.934337558 16.302030865
Ag 2.934105249 2.931047466 16.305752088
Ag 5.864684423 2.919209777 16.303161352
Ag 8.799317190 2.929385420 16.305478865
Ag 0.008860579 5.863696629 16.304745655
Ag 2.933296057 5.862725672 16.304576336
Ag 5.870071860 5.858756826 16.312588496
Ag 8.810088991 5.863188168 16.302694046
Ag 0.001616440 8.793126052 16.301839655
Ag 2.935342054 8.793590947 16.306231729
Ag 5.865062867 8.795453619 16.303339021
Ag 8.798635196 8.795782160 16.305838392

C 3.37814179 6.39239217 24.88549987
C 3.36984357 5.13109555 24.26478657
C 3.73586065 5.02312103 22.92847463
C 4.11658181 6.14977698 22.18543343
C 4.12968665 7.39905626 22.82355632
C 3.76730245 7.53040938 24.15857723
H 3.06654171 4.25219039 24.82947752
H 3.70531734 4.04513479 22.44722725
H 4.40945130 8.28875455 22.25917483
H 3.77152115 8.50583749 24.64048186
C 2.96439325 6.52155016 26.24150919
C 4.52217354 6.02223647 20.72821349
H 3.95266067 5.20182610 20.26833580
H 4.25431582 6.94948387 20.20118452
N 5.94527713 5.76604622 20.47346079
C 6.82793612 6.84838788 20.88199073
H 6.90345464 6.97086848 21.98214195
H 7.83905956 6.65162923 20.50076695
H 6.47618326 7.79779240 20.45580265
C 6.41010143 4.46732628 20.93672436
H 7.42419859 4.29113124 20.55325195
H 6.44974769 4.37466175 22.04183919
H 5.75295919 3.67689332 20.54937237
N 2.61756589 6.62860632 27.34855249

Environ input file, Ag (100)

```
&ENVIRON
  verbose = 2
  environ_thr = 1.d-1
  environ_type = 'input'
  ! env_electrostatic = .true.
  env_static_permittivity = 47.0D0
  env_dielectric_regions = 1
/
&BOUNDARY
  solvent_mode = 'electronic'
 /
&ELECTROSTATIC
  !
  pbc_correction = 'none'
  pbc_dim = 3
  ! pbc_axis = 3
  !
  tol = 1.d-11
  mix = 0.6
  solver = 'iterative'
  auxiliary = 'full'
  !
/
```

```
DIELECTRIC_REGIONS {angstrom}
1.0   1.0   5.5   5.5   8.2800   8.00   0.5   2   3
```

Environ input file, Ag (111)

```
&ENVIRON
  verbose = 2
  environ_thr = 1.d-1
  environ_type = 'input'
  env_static_permittivity = 47.0D0
  env_dielectric_regions = 1
/
&BOUNDARY
  solvent_mode = 'electronic'
 /
&ELECTROSTATIC
  !
  pbc_correction = 'none'
  pbc_dim = 3
  ! pbc_axis = 3
  !
  tol = 1.d-11
  mix = 0.6
  solver = 'iterative'
  auxiliary = 'full'
  !
/
DIELECTRIC_REGIONS {angstrom}
1.0   1.0   5.5   5.5   8.2800   8.00   0.5   2   3
```

Environ input file, Ag (322)

```
&ENVIRON
  verbose = 2
  environ_thr = 1.d-1
  environ_type = 'input'
  ! env_electrostatic = .true.
  env_static_permittivity = 47.0D0
  env_dielectric_regions = 1
/
&BOUNDARY
  solvent_mode = 'electronic'
 /
&ELECTROSTATIC
  !
  pbc_correction = 'none'
  pbc_dim = 3
  ! pbc_axis = 3
  !
  tol = 1.d-11
  mix = 0.6
  solver = 'iterative'
  auxiliary = 'full'
```

```
   !
/
DIELECTRIC_REGIONS {angstrom}
1.0   1.0   5.5   5.5   8.2800   8.00   0.5   2   3
```

Phonon input file, MAMBN

```
Vibrational modes of molecule (gamma pt phonon calc)
 &inputph
  outdir='./',
  prefix='teah',
  amass(1)=14.007,
  amass(2)=12.011,
  amass(3)=1.008,
  fildyn='teah.dynG',
  trans= .true.
  nogg = .true.
  asr = .true.
  tr2_ph=1d-17
 /
0.0 0.0 0.0
```

Cyclic Voltammetry

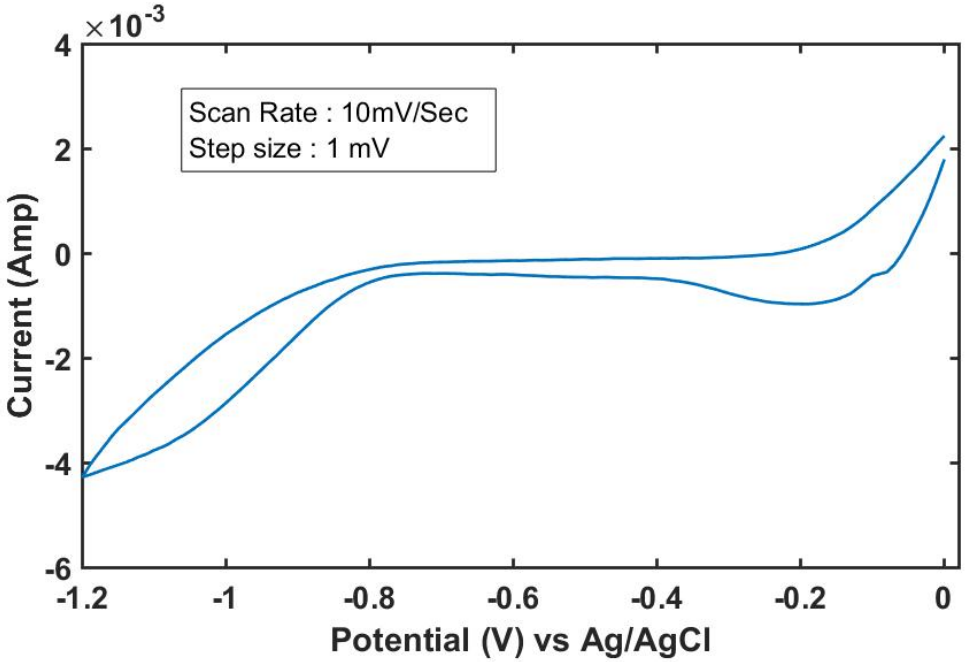

Figure S10. Cyclic voltammogram (10 mV s^{-1}) of polycrystalline silver recorded in DMSO containing 100 mM MAMBN-H^+ (reactant), and 300mM tetrabutylammonium hexafluorophosphate (supporting electrolyte)

Open Circuit Potential (OCP) Measurement to Determine the Equilibrium Potential of Triethyl Amine and Triethyl Ammonium Redox Couple

We followed the procedure described previously[35] to measure the equilibrium potential for the triethylamine/triethylammonium couple, which is closely related to the redox couple studied in this work. 50 mM Triethylamine and 125 mM triethyl ammonium chloride were used as stock solution. 300 mM tetrabutylammonium hexafluorophosphate (as supporting electrolyte), 2.5 M 1:1 Pyridine: Pyridinium chloride (as buffer, to overcome the hydrogen bonding effect within the redox couple) were added to both the stock solutions. DMSO was used as solvent. To a 10 ml solution of 50 mM triethyl amine, 500 µl of 125 mM triethyl ammonium chloride solution was added successively, and open circuit potential was measured after each addition using Gamry Reference 3000 potentiostat. In this measurement, Ag/AgCl was used as reference electrode and 250 µm silver foil as working electrode. Data was recorded every 1 second over a duration of 10 minutes for each addition of the protonated species. Stability of the measurements was set such that the drift of the potential is not more than 0.005 mV/s. There was continuous N_2 flow and stirring at a constant rate during the experiment. Before using as the working electrode in the OCP experiment, the silver foil was held at -0.5 V for ~3 minutes in 3 M KCl solution to remove trace amount of silver oxide, if any.

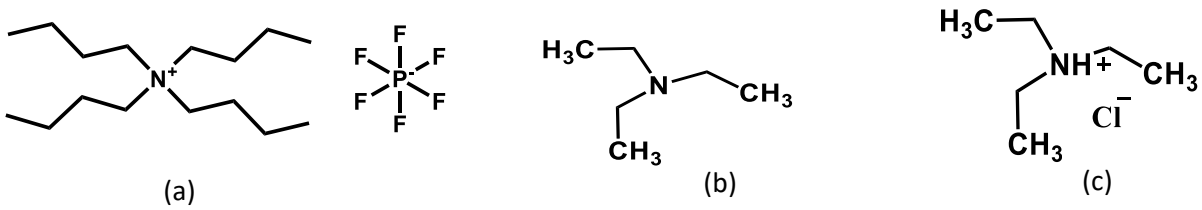

Figure S11. (a) The supporting electrolyte. (b,c) The redox couple.

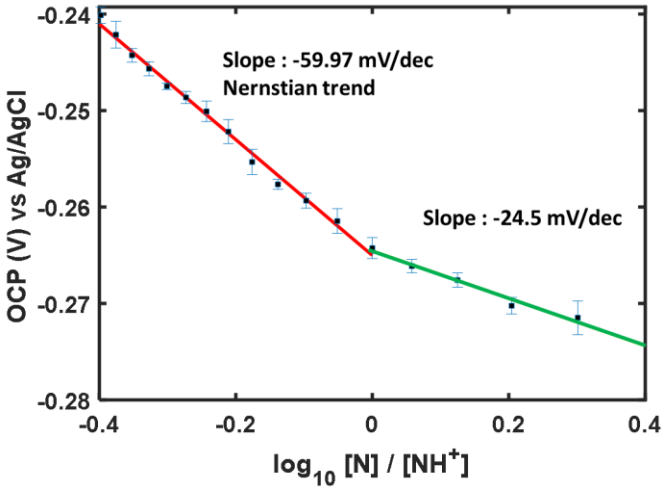

Figure S12. The open circuit potential as a function of the log of concentration ratio of the deprotonated and protonated species.

From each of the OCP vs time plots, potential values are averaged over last 5 minutes and used to make OCP vs mole-ratio plot (Figure S12). The reaction potential can be obtained using the following:[35]

$$E = E^0 - \frac{0.0592}{n} log \frac{[Et_3N]}{[Et_3N^+]} - \frac{0.0592}{n} log \frac{[Pyr]}{[PyrH^+]} - 0.0592\, pK_a$$

The potential at 1:1 mole ratio of the protonated and deprotonated species represents the Y-intercept of Figure S12:

$$E = E^0 - 0.0592\, pK_a$$

The Nernstian portion of the data in the figure and the pK_a of pyridine/pyridinium buffer in DMSO[36] was used to estimate E^0.

$E^0 = 0.05997 pK_a$ + Y-intercept = 0.05997*3.4 -0.26501 = -0.0611 V

References

1. Giannozzi, P., et al., Quantum Espresso: A Modular and Open-Source Software Project for Quantum Simulations of Materials. *J. Phys.: Condens. Matter* **2009**, *21*, 395502.
2. Giannozzi, P., et al., Advanced Capabilities for Materials Modelling with Quantum Espresso. *J. Phys.: Condens. Matter* **2017**, *29*, 465901.
3. Perdew, J. P.; Burke, K.; Ernzerhof, M., Generalized Gradient Approximation Made Simple. *Phys. Rev. Lett.* **1996**, *77*, 3865-3868.
4. Grimme, S.; Antony, J.; Ehrlich, S.; Krieg, H., A Consistent and Accurate Ab Initio Parametrization of Density Functional Dispersion Correction (Dft-D) for the 94 Elements H-Pu. *J. Chem. Phys* **2010**, *132*, 154104.
5. Tonigold, K.; Groß, A., Dispersive Interactions in Water Bilayers at Metallic Surfaces: A Comparison of the Pbe and Rpbe Functional Including Semiempirical Dispersion Corrections. *J. Comput. Chem.* **2012**, *33*, 695-701.
6. Hamann, D. R., Optimized Norm-Conserving Vanderbilt Pseudopotentials. *Phys. Rev. B* **2013**, *88*, 085117.
7. Schlipf, M.; Gygi, F., Optimization Algorithm for the Generation of Oncv Pseudopotentials. *Comput. Phys. Commun.* **2015**, *196*, 36-44.
8. Methfessel, M.; Paxton, A. T., High-Precision Sampling for Brillouin-Zone Integration in Metals. *Phys. Rev. B* **1989**, *40*, 3616-3621.
9. Andreussi, O.; Dabo, I.; Marzari, N., Revised Self-Consistent Continuum Solvation in Electronic-Structure Calculations. *J. Chem. Phys* **2012**, *136*, 064102.
10. Lu, Z.; Manias, E.; Macdonald, D. D.; Lanagan, M., Dielectric Relaxation in Dimethyl Sulfoxide/Water Mixtures Studied by Microwave Dielectric Relaxation Spectroscopy. *J. Phys. Chem. A* **2009**, *113*, 12207-12214.
11. Goldsmith, Z. K.; Secor, M.; Hammes-Schiffer, S., Inhomogeneity of Interfacial Electric Fields at Vibrational Probes on Electrode Surfaces. *ACS Cent. Sci.* **2020**, *6*, 304-311.
12. Fumagalli, L., et al., Anomalously Low Dielectric Constant of Confined Water. *Science* **2018**, *360*, 1339.
13. Wasserman, H. J.; Vermaak, J. S., On the Determination of a Lattice Contraction in Very Small Silver Particles. *Surf. Sci.* **1970**, *22*, 164-172.
14. Stachiotti, M. G., First-Principles Study of the Adsorption of ${\Text{Nh}}_{3}$ on Ag Surfaces. *Phys. Rev. B* **2009**, *79*, 115405.

15. Martínez, A., Bonding Interactions of Metal Clusters [Mn (M= Cu, Ag, Au; N=1-4)] with Ammonia. Are the Metal Clusters Adequate as a Model of Surfaces? *J. Braz. Chem. Soc.* **2005**, *16*, 337-344.
16. Dronskowski, R.; Bloechl, P. E., Crystal Orbital Hamilton Populations (Cohp): Energy-Resolved Visualization of Chemical Bonding in Solids Based on Density-Functional Calculations. *The Journal of Physical Chemistry* **1993**, *97*, 8617-8624.
17. Deringer, V. L.; Tchougréeff, A. L.; Dronskowski, R., Crystal Orbital Hamilton Population (Cohp) Analysis as Projected from Plane-Wave Basis Sets. *J. Phys. Chem. A* **2011**, *115*, 5461-5466.
18. Maintz, S.; Esser, M.; Dronskowski, R., Efficient Rotation of Local Basis Functions Using Real Spherical Harmonics. *Acta Phys. Pol., B* **2016**, *47*, 1165.
19. Maintz, S.; Deringer, V. L.; Tchougréeff, A. L.; Dronskowski, R., Analytic Projection from Plane-Wave and Paw Wavefunctions and Application to Chemical-Bonding Analysis in Solids. *J. Comput. Chem.* **2013**, *34*, 2557-2567.
20. Maintz, S.; Deringer, V. L.; Tchougréeff, A. L.; Dronskowski, R., Lobster: A Tool to Extract Chemical Bonding from Plane-Wave Based Dft. *J. Comput. Chem.* **2016**, *37*, 1030-1035.
21. Hörmann, N. G.; Guo, Z.; Ambrosio, F.; Andreussi, O.; Pasquarello, A.; Marzari, N., Absolute Band Alignment at Semiconductor-Water Interfaces Using Explicit and Implicit Descriptions for Liquid Water. *npj Computational Materials* **2019**, *5*, 100.
22. Ives, D. J. G.; Janz, G. J., *Reference Electrodes, Theory and Practice*; Academic Press: New York, 1961.
23. Frisch, M. J.; Pople, J. A.; Binkley, J. S., Self-Consistent Molecular Orbital Methods 25. Supplementary Functions for Gaussian Basis Sets. *J. Chem. Phys* **1984**, *80*, 3265-3269.
24. Clark, T.; Chandrasekhar, J.; Spitznagel, G. W.; Schleyer, P. V. R., Efficient Diffuse Function-Augmented Basis Sets for Anion Calculations. Iii. The 3-21+G Basis Set for First-Row Elements, Li–F. *J. Comput. Chem.* **1983**, *4*, 294-301.
25. Ditchfield, R.; Hehre, W. J.; Pople, J. A., Self-Consistent Molecular-Orbital Methods. Ix. An Extended Gaussian-Type Basis for Molecular-Orbital Studies of Organic Molecules. *J. Chem. Phys* **1971**, *54*, 724-728.
26. Hehre, W. J.; Ditchfield, R.; Pople, J. A., Self—Consistent Molecular Orbital Methods. Xii. Further Extensions of Gaussian—Type Basis Sets for Use in Molecular Orbital Studies of Organic Molecules. *J. Chem. Phys* **1972**, *56*, 2257-2261.
27. Becke, A. D., Density-Functional Thermochemistry. Iii. The Role of Exact Exchange. *J. Chem. Phys* **1993**, *98*, 5648-5652.
28. Stephens, P. J.; Devlin, F. J.; Chabalowski, C. F.; Frisch, M. J., Ab Initio Calculation of Vibrational Absorption and Circular Dichroism Spectra Using Density Functional Force Fields. *The Journal of Physical Chemistry* **1994**, *98*, 11623-11627.
29. Chai, J.-D.; Head-Gordon, M., Long-Range Corrected Hybrid Density Functionals with Damped Atom–Atom Dispersion Corrections. *Phys. Chem. Chem. Phys.* **2008**, *10*, 6615-6620.
30. Frisch, M. J., et al. *Gaussian 16 Rev. C.01*, Wallingford, CT, 2016.
31. Marston, C. C.; Balint-Kurti, G. G., The Fourier Grid Hamiltonian Method for Bound State Eigenvalues and Eigenfunctions. *J. Chem. Phys* **1989**, *91*, 3571-3576.
32. Tang, W.; Sanville, E.; Henkelman, G., A Grid-Based Bader Analysis Algorithm without Lattice Bias. *J. Phys.: Condens. Matter* **2009**, *21*, 084204.
33. Sanville, E.; Kenny, S. D.; Smith, R.; Henkelman, G., Improved Grid-Based Algorithm for Bader Charge Allocation. *J. Comput. Chem.* **2007**, *28*, 899-908.
34. Henkelman, G.; Arnaldsson, A.; Jónsson, H., A Fast and Robust Algorithm for Bader Decomposition of Charge Density. *Comput. Mater. Sci* **2006**, *36*, 354-360.
35. Wise, C. F.; Agarwal, R. G.; Mayer, J. M., Determining Proton-Coupled Standard Potentials and X–H Bond Dissociation Free Energies in Nonaqueous Solvents Using Open-Circuit Potential Measurements. *J. Am. Chem. Soc.* **2020**, *142*, 10681-10691.

36. Tshepelevitsh, S.; Kütt, A.; Lõkov, M.; Kaljurand, I.; Saame, J.; Heering, A.; Plieger, P. G.; Vianello, R.; Leito, I., On the Basicity of Organic Bases in Different Media. *Eur. J. Org. Chem.* **2019**, *2019*, 6735-6748.